The Journal of Immunology

RESEARCH ARTICLE | JANUARY 01 2019

Improved Multiplex Immunohistochemistry for Immune Microenvironment Evaluation of Mouse Formalin-Fixed, Paraffin-Embedded Tissues

Noah Sorrelle; ... et. al

J Immunol (2019) 202 (1): 292–299.
https://doi.org/10.4049/jimmunol.1800878

Improved Multiplex Immunohistochemistry for Immune Microenvironment Evaluation of Mouse Formalin-Fixed, Paraffin-Embedded Tissues

Noah Sorrelle,*[,1] Debolina Ganguly,*[,1] Adrian T. A. Dominguez,* Yuqing Zhang,* Huocong Huang,* Lekh N. Dahal,[†] Natalie Burton,* Arturas Ziemys,[‡] and Rolf A. Brekken*[,§]

Immune profiling of tissue through multiplex immunohistochemistry is important for the investigation of immune cell dynamics, and it can contribute to disease prognosis and evaluation of treatment response in cancer patients. However, protocols for mouse formalin-fixed, paraffin-embedded tissue have been less successful. Given that formalin fixation and paraffin embedding remains the most common preparation method for processing mouse tissue, this has limited the options to study the immune system and the impact of novel therapeutics in preclinical models. In an attempt to address this, we developed an improved immunohistochemistry protocol with a more effective Ag-retrieval buffer. We also validated 22 Abs specific for mouse immune cell markers to distinguish B cells, T cells, NK cells, macrophages, dendritic cells, and neutrophils. In addition, we designed and tested novel strategies to identify immune cells for which unique Abs are currently not available. Last, in the 4T1 model of breast cancer, we demonstrate the utility of our protocol and Ab panels in the quantitation and spatial distribution of immune cells. ***The Journal of Immunology*****, 2019, 202: 292–299.**

Using immunohistochemistry (IHC) to evaluate immune cell dynamics in vivo complements immunophenotyping via flow cytometry (1, 2), providing a method for validation. Further, with the advent of immunotherapy to treat cancer and other diseases, it has become increasingly important to evaluate infiltrating immune cells in the context of the whole tissue (3–5). Determining the tissue distribution of specific Ags, especially immune markers, is necessary for the diagnosis and investigation of disease. In cancer, this can assist in the understanding of immune cell behavior in the tumor microenvironment at primary and metastatic sites (6, 7).

Although multiple groups have made strides regarding multiplex IHC of human tissues for immune cell characterization (8–10), protocols using mouse formalin-fixed, paraffin-embedded (FFPE) tissues are still underdeveloped. Many epitopes are formalin fixation–sensitive and not easily detected. Historically, detection of formalin-sensitive epitopes has relied on frozen tissue (11, 12), which comes with the disadvantage of cumbersome storage and compromised tissue morphology.

Zinc salt fixation has been proposed as an alternative to formalin fixation as a strategy to retain tissue morphology while resulting in less epitope masking (13, 14). Zinc salt fixation may indeed have advantages; however, there are only limited IHC studies comparing the two fixation methods. Additionally, there are concerns that zinc-based fixatives may not penetrate tissues as effectively as formalin (15). Further, to the best of our knowledge, the long-term stability of zinc-fixed tissue is unreported. Finally, formalin fixation remains the most common fixation method for mouse tissues.

In this study, we demonstrate multiplex IHC of mouse immune cell markers with an improved Ag retrieval protocol that works efficiently for most Abs. We used specific markers to detect populations of B cells, subtypes of T cells, NK cells, macrophages, dendritic cells (DCs), granulocytes, and total myeloid cells. We assessed Ab specificity by using tissue from wild-type, SCID, NOD SCID γ (NSG), and control- or clodronate liposome–treated mice. Finally, we demonstrate the utility of the protocol in evaluating the immune landscape in a preclinical model of breast cancer.

Materials and Methods

All materials are available from commercial sources or can be derived using methods described in this study. All relevant data are reported in the article.

Mice

Male and female BALB/c (BALB/cfC3H strain) and SCID mice were purchased from the on-campus University of Texas (UT) Southwestern

*Division of Surgical Oncology, Department of Surgery, Hamon Center for Therapeutic Oncology Research, University of Texas Southwestern Medical Center, Dallas, TX 75390; [†]Centre for Cancer Immunology, Faculty of Medicine, Southampton General Hospital, University of Southampton, Southampton 016 6YD, United Kingdom; [‡]Department of Nanomedicine, Houston Methodist Research Institute, Houston, TX 77030; and [§]Department of Pharmacology, University of Texas Southwestern Medical Center, Dallas, TX 75390

[1]N.S. and D.G. contributed equally to this work.

ORCIDs: 0000-0002-4576-3912 (N.S.); 0000-0002-7184-0053 (D.G.); 0000-0003-3387-7805 (A.T.A.D.); 0000-0002-6345-4566 (H.H.); 0000-0001-8390-6593 (L.N.D.); 0000-0001-5366-0510 (N.B.); 0000-0003-2704-2377 (R.A.B.).

Received for publication June 25, 2018. Accepted for publication October 29, 2018.

This work was supported by National Institutes of Health Grants R01 CA192381 (to R.A.B.), U54 CA210181 (to R.A.B. and A.Z., M. Ferrari, principal investigator), and F31 CA19603301 (to N.S.) and an Effie Marie Cain scholarship in angiogenesis research (to R.A.B.). L.N.D. was funded by Bloodwise Programme Grant 12050.

Author contributions: conception and design, N.S. and D.G.; development of methodology, N.S. and D.G.; acquisition of data, N.S., D.G., A.T.A.D., Y.Z., H.H., L.N.D., and N.B.; analysis and interpretation of data, N.S., D.G., A.Z., R.A.B.; administrative, technical, and material support, R.A.B.; and study supervision: R.A.B.

The funders had no role in study design, data collection and analysis, decision to publish, or preparation of the manuscript.

Address correspondence and reprint requests to Prof. Rolf A. Brekken, University of Texas Southwestern Medical Center, 6000 Harry Hines Boulevard, Dallas, TX 75390-8593. E-mail address: rolf.brekken@utsouthwestern.edu

The online version of this article contains supplemental material.

Abbreviations used in this article: AP, alkaline phosphatase; DC, dendritic cell; FFPE, formalin-fixed, paraffin-embedded; HIER, heat-induced epitope retrieval; IHC, immunohistochemistry; MHCII, MHC class II; NSG, NOD SCID γ; PBSt, PBS with Tween; TSA, tyramide signal amplification; UT, University of Texas.

Mouse Breeding Core (Dallas, TX). Tissue from NSG mice was a kind gift from Dr. S. Morrison (UT Southwestern Medical Center). All animals were housed in a pathogen-free environment with access to food and water ad libitum.

Macrophage depletion

Control ("Encapsomes") and clodronate liposomes ("Clodrosomes") were obtained from Encapsula NanoSciences (Brentwood, TN). Eight-week-old BALB/c male mice were injected i.p. with 300 μl of Encapsomes (control) or Clodrosomes. Mice were euthanized 72 h postinjection, and tissues were fixed in 10% neutral-buffered formalin for 48 h before embedding in paraffin.

Cells

The 4T1 breast cancer cells were obtained from the American Type Culture Collection (Manassas, VA). The cells were cultured in DMEM (Sigma-Aldrich) supplemented with 10% FCS (Rocky Mountain Biologicals) at 37˚C in a humid atmosphere with 5% CO_2.

4T1 breast cancer model

The 4T1 cells (10^5) were injected orthotopically into the inguinal mammary fat pat of 8-wk-old female BALB/c mice. Mice were euthanized 3 wk postinjection. The established tumor was resected and fixed in 10% neutral-buffered formalin for 48 h before embedding in paraffin. All experiments were approved by the Institutional Animal Care and Use Committee at UT Southwestern and conducted in accordance with an approved protocol.

Immunohistochemistry

Tissue fixation. All tissues were fixed in 10% neutral buffered formalin for 48 h on a shaker at room temperature. Tissues were washed and stored in PBS at 4˚C until embedded. Paraffin embedding was performed by the UT Southwestern Molecular Pathology Core.

Tissue sectioning. Before sectioning, FFPE tissue blocks were incubated in 70% ethanol with 10% glycerol for 5 min to soften, followed by a quick rinse in distilled water. Then, 5-μm sections were cut using a Leitz 1512 Rotary Microtome and placed onto a water bath at 40˚C for 2 min to reduce wrinkles. Sections were transferred to positively charged slides (no. SFH1103; Biocare Medical) and allowed to dry overnight before staining.

Deparaffinization, staining, and imaging. Slides were warmed for 10 min in a 60˚C oven before following the deparaffinization protocol. The deparaffinization and rehydration protocol entails incubation in xylene (3× for 5 min), 100% ethanol (2× for 2 min), 95% ethanol (2× for 2 min), 70% ethanol (2× for 2 min), 50% ethanol (2× for 2 min), and PBS (1× 3 min). To prevent sections from folding or falling off the slides during Ag retrieval and Ab stripping, the deparaffinized slides were fixed in 10% neutral buffered formalin for 30 min, followed by incubation in PBS (2× for 3 min).

For Ag retrieval, 250 ml of Ag retrieval buffer (10 mM Tris-HCl and 1 mM EDTA with 10% glycerol [pH 9]) was preheated to 80˚C in a bucket inside a pressure cooker (Biocare Medical) filled with 500 ml of water. Slides were then placed inside the buffer and heated at 110˚C for 18 min (~4–5ψ). Slides were allowed to cool at room temperature for 30 min, followed by a PBS rinse. Tissue sections were surrounded by a hydrophobic barrier using a PAP pen and blocked for 10 min with 2.5% goat serum and 2.5% horse serum (Vector Laboratories) or for 30 min with Rodent Block M (Biocare Medical) if the secondary host was goat, horse, or rat, respectively.

Incubation with primary Ab was performed on a shaker for 1 h at room temperature or at 4˚C overnight. Slides were washed in PBS with Tween (PBSt; 0.05% Tween 20 plus 2 mM EDTA; 3× for 5 min) before adding the "polymer" HRP- or alkaline phosphatase (AP)-conjugated secondary Abs (ImmPRESS; Vector Laboratories). Sections were incubated with secondary Ab for 30 min on a shaker, followed by one PBSt (0.2% Tween 20 plus 2 mM EDTA) and two PBSt (0.05% Tween 20 plus 2 mM EDTA) washes, 5 min each. Sections were then incubated with chromogenic or tyramide signal amplification (TSA) substrates. For multiplex staining, Ab stripping was performed in 10 mM citrate buffer (pH 6.2) plus 10% glycerol in a pressure cooker at 110˚C for 2 min before probing with the next primary Ab.

For chromogenic detection, Betazoid DAB, Warp Red, and Ferangi Blue (BDB2004L, WR806S, and FB813H, respectively; Biocare Medical) were used. Substrate incubation time was determined by monitoring signal development using a microscope. After developing with chromogenic substrates, slides were counterstained with hematoxylin. Bluing was performed by running tap water over the slides for 30 s. Slides were coverslipped using VectaMount (H-5501; Vector Laboratories) and scanned at 20× using the Hamamatsu NanoZoomer 2.0-HT.

For fluorescence detection, we used a TSA detection system (PerkinElmer). The following fluorophores were used: OPAL 520, OPAL 570, and OPAL 690. DAPI was used for nuclear counterstaining. To reduce the autofluorescence, slides were incubated at the end in TrueBlack Lipofuscin Autofluorescence Quencher (no. 23007; Biotium) diluted 20-fold in 70% ethanol for 30 s. Slides were coverslipped using ProLong Gold (no. P36931; Life Technologies). Slides were scanned at 20× using the Zeiss Axio Scan.Z1 (Whole Brain Microscopy Facility, UT Southwestern). DAPI, AF488 (for OPAL 520), AF555 (for OPAL 570), and AF660 (for OPAL 690) channels were used to acquire images. The exposure time for image acquisition was between 5 and 100 ms.

IHC Abs. Primary Abs were diluted in PBSt (0.05%) plus 2 mM EDTA plus 0.5% serum (goat or horse, based on the host of the secondary Ab), or Renaissance Background Reducing Diluent (PD905; Biocare Medical) when incubating sections with more than one primary Ab simultaneously. The primary Abs and dilution factors used are displayed in Table I. Polymer secondary Abs were purchased from Vector Laboratories (ImmPRESS HRP anti-rabbit IgG [no. MP-7401], HRP anti-rat IgG [no. MP-7404], AP anti-rat IgG [no. MP-5404], and AP anti-rabbit IgG [no. MP-5401]).

Flow cytometry

Single-cell suspensions were prepared from C57BL/6 mouse spleens. The 1×10^6 cells were stained with CD11b PE, Ly6C PerCP-Cy5.5, Ly6G PE-Cy7 (eBioscience), F4/80 APC (Bio-Rad AbD Serotec Limited), and FcγR Abs as previously described (16, 17). Data were acquired on the FACSCanto II (BD Biosciences) and analyzed with FCS Express (De Novo Software). FcγR expression by macrophages ($F4/80^+$), monocytes ($CD11b^+Ly6C^+$), and neutrophils ($CD11b^+Ly6G^+$) is demonstrated by mean fluorescence intensity.

Image analysis

Image analysis was conducted using Fiji software (18). During the analysis, eight-bit images were thresholded at the same intensity value for a specific staining (e.g., CD3, CD11c, etc.) and converted to binary format. To calculate tissue areas that are double-stained or have specific staining patterns (e.g., $CD8^+$ and $CD4^-$), an "Image Calculator Function" was used. Then, the area fraction of the signal in resulting binary images was calculated. All calculated area fractions of different staining were normalized using DAPI.

Results

We sought to develop an improved protocol for IHC on mouse FFPE sections with the following requirements: 1) reproducibility of staining across different tissues from different experiments; 2) consistent results with most Abs used without laborious Ab-specific Ag retrieval optimization; and 3) ability to perform multiplex IHC.

In accord with previous reports, we found that Tris/EDTA (pH 9) Ag retrieval buffer was optimal for most primary Abs (19). Further, we found that the addition of 10% glycerol significantly enhanced Ag retrieval in multiple cases (Supplemental Fig. 1A–L). Additionally, we found that adding a short 10% neutral buffered formalin fixation step after deparaffinization prevented tissue folding, which can be an issue with higher pH buffers during heat-induced epitope retrieval (HIER). This did not impact epitope detection (data not shown).

For Ab stripping, some groups use a short HIER-like step in citrate buffer (pH 6.2), whereas others have reported success with incubating the slides in a 100-mM glycine/Tween 20 buffer (pH 10) at room temperature (14). We found that the glycine buffer–based stripping method failed to remove the primary Ab (Supplemental Fig. 1N, 1Q). In contrast, the short HIER-like step in citrate buffer worked effectively (Supplemental Fig. 1O, 1R). We suspect heat denaturing of high-affinity Abs is particularly important in this process.

To demonstrate consistency across detection methods, we first performed single staining on spleens using three different Abs, starting with fluorescence (TSA) detection. Following a stripping step, we reprobed the same tissue with the same Abs and used chromagen detection (Supplemental Fig. 2). Cells were stained identically with each method.

Table I. Primary Abs and dilution factors

Target/Ab	Alias(es)	Company	Catalog Number	Clone	Dilution Factor, Chromogen Staining	Dilution Factor, Fluorescent (TSA) Staining
CD11b	Itgam	Abcam	ab133357	EPR1344	5000	20000
CD11c	Itgax	Cell Signaling	97585S	D1V9Y	100	200
CD163	M130	Abcam	ab182422	EPR19518	6000	12000
CD19		Cell Signaling	90176	D4V4B	1000	2000
CD3e		Thermo Fisher Scientific	PA1-29547	Polyclonal	1000	3000
CD3e[a]		Abcam	ab11089	CD3-12	250	750
CD4		Sino Biological	50134-R001	Clone ID: 1	1000	3000
CD4		Abcam	ab183685	EPR19514	2000	8000
CD8a	Lyt2	Cell Signaling	98941	D4W2Z	4000	8000
Eomes	Tbr2	Abcam	ab183991	EPR19012	500	ND
F4/80	Emr1, Adgre1	Cell Signaling	70076	D2S9R	500	1000
F4/80	Emr1, Adgre1	Thermo Fisher Scientific	MA5-16363	SP115	500	800
FcgR1	CD64	Sino Biological	50086-R008-50	Clone ID: 8	5000	10000
FcgR4	CD16-2	Sino Biological	50036-R011-50	Clone ID: 11	2000	2500
Foxp3		R&D Systems	MAB8214	1054C	500	2000
Granzyme B	Gzmb, Ctla1	Cell Signaling	46890	D6E9W	500	ND
MHCII (IA/IE)	H2-Ab1	BioLegend	107601	M5/114.15.2	200	500
Ox40	Tnfrsf4	Cell Signaling	61637	E9U70	500	ND
Pax5	BSAP	Abcam	ab109443	EPR3730	1000	2000
PD1	Pdcd1	Cell Signaling	846S1T	D7DSW	200	ND
S100a9	MRP14, CAGB	Cell Signaling	73425S	D3U8M	1000	4000
Zap70	Srk	Cell Signaling	2705	99F2	500	500

[a]This Ab does not work well for combined TSA staining with CD4 and CD8; staining with CD3 first prevents subsequent staining for CD4 or CD8 on $CD3^+$ cells and vice versa.

To evaluate the effect of the stripping step on Ag retrieval, we stained spleens after the primary Ag retrieval step ("Round 1," Supplemental Fig. 3). Second, we stained different spleen sections for the same markers after performing Ag retrieval and a single stripping step ("Round 2," Supplemental Fig. 3). Third, we repeated this on spleens that were subjected to Ag retrieval and two subsequent stripping steps ("Round 3," Supplemental Fig. 3). For the three Abs tested on spleens (CD3, CD19, and Pax5), we did not observe significant differences in detection before or after the tissue was exposed to multiple stripping steps. However, this is not the case for every Ab/epitope (e.g., F4/80 [D2S9R]; Supplemental Fig. 3K, 3L). Thus, laboratories should perform such testing to determine the order of staining for multiplex protocols involving Ab stripping steps.

After the primary Ag retrieval step and multiple iterations of stripping in multiplex staining, we found that the nuclear signal, via DAPI or hematoxylin, is lost if the staining is done over a longer timeframe (hours versus days; data not shown). We suspect that nuclear DNA is vulnerable to environmental DNase contamination after extensive destruction of formalin cross-links. This issue was resolved by adding EDTA to wash buffers and Ab diluents.

Applying our revised protocol, we tested over 35 primary Abs specific for mouse immune subsets and developed a panel of lymphoid and myeloid cell markers (Table I). These markers were chosen based on ImmGen expression data (Fig. 1) (20), previous reports (16, 17, 21–24), and Ab availability. Using chromagen and fluorescence (via TSA) detection methods, we observed that each marker produced expected staining patterns corresponding with known localization and expression by the respective cell types of interest (Supplemental Fig. 4) (25).

To validate Ab specificity, we used two strategies. First, we stained tissue in which cell types/markers of interest are expected to be decreased compared to control tissue. For the lymphoid panel, we stained spleens from wild-type, SCID, and NSG mice (Fig. 2A–G1). Compared to wild-type, we observed a decrease in lymphoid cell markers in SCID and NSG spleens. For example, CD3 and CD19 (T cell and B cell markers, respectively) are completely absent in SCID and NSG tissue. As a positive control, CD11b, mostly a myeloid-lineage marker, was consistent across all groups (Fig. 2B1–D1).

To test macrophage markers, we stained livers from control- or clodronate liposome–treated mice, as clodronate liposomes deplete professional phagocytic cells, primarily macrophages (26, 27). Macrophage staining was markedly reduced in clodronate liposome–treated mice (Fig. 2H1–Q1).

For our second strategy to confirm Ab specificity, we used multiple Abs for the same marker or cell type when possible. For example, we used two different Abs for F4/80 (Fig. 2H1–K1). For B cells, we used two different B cell–specific markers, CD19 and Pax5 (Fig. 2J–O).

When developing the Ab panels, we found that for some cell types (e.g., DCs, neutrophils, and NK cells), Abs for cell-specific markers were not available. To address this, we used multimarker staining strategies.

For example, we developed a strategy to stain NK cells using CD3 and Zap70. *CD3* is expressed by T cells, but not NK cells (Fig. 1) (20). *Zap70* is expressed by T cells and NK cells (Fig. 1) (20). Because SCID and NSG mice lack T cells, CD3 staining is absent in SCID and NSG spleens compared with wild-type (Fig. 2A–C). In contrast, some $Zap70^+$ cells remain, presumably NK cells (Fig. 2D–F). Combining these markers, we stained spleens for CD3 and Zap70 using both chromagen and fluorescence detection methods, demonstrating the presence of $CD3^+Zap70^+$ and $CD3^-Zap70^+$ cells, corresponding to T cells and NK cells, respectively (Fig. 3A, 3B). In the case of chromagen staining, we first stained for CD3 using a dark brown chromagen (diaminobenzidine), intentionally obscuring further staining wherever the chromagen is deposited. We subsequently performed Zap70 staining using a red chromagen (Warp Red). Through this strategy, it is easy to identify Zap70 single positive cells using chromagen detection (Fig. 2A, inset).

We also developed a strategy to detect DCs. Although *CD11c* has long been used as a DC marker, it is not cell type exclusive, as it is may be expressed by macrophage subsets and other immune cells (Fig. 1) (20). MHC class II (MHCII; *H2-Ab1*) is also not exclusive, but it is expressed more consistently across DC subsets and is found on fewer cell types (Fig. 1) (20). Because MHCII is

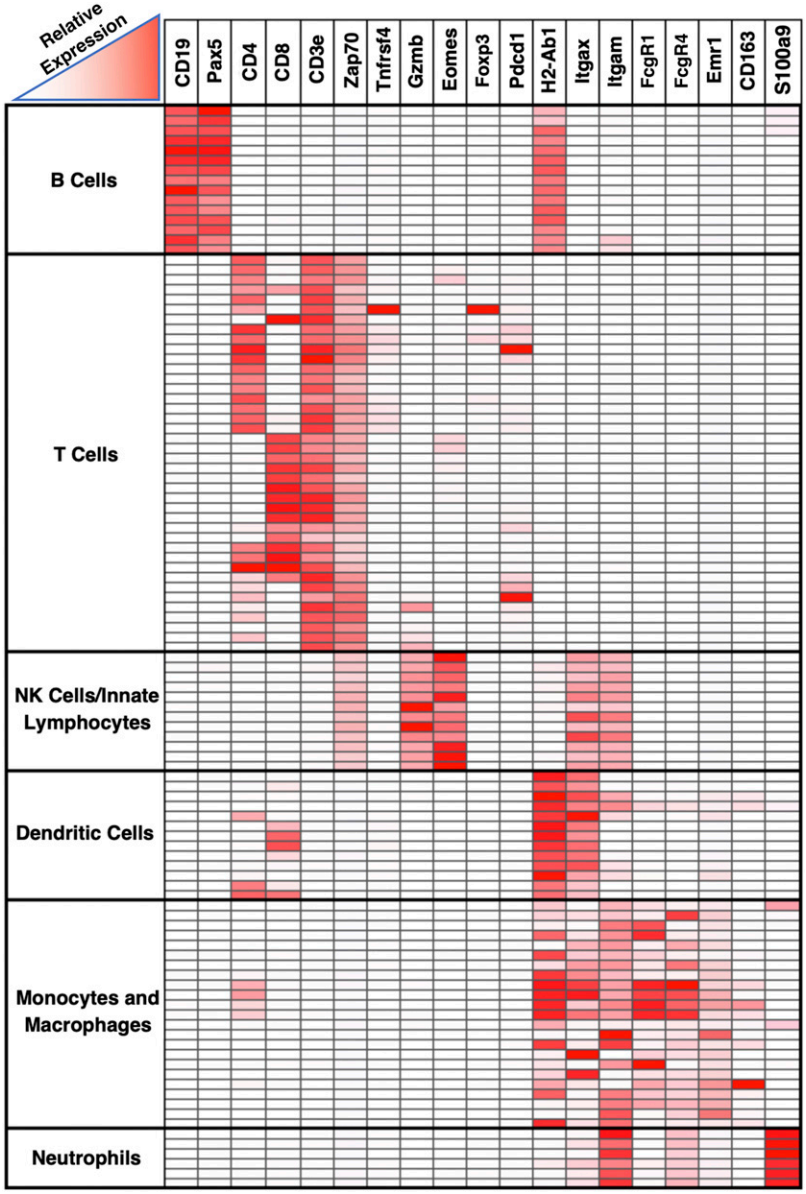

FIGURE 1. Heatmap depicting immune cell expression of markers used in our IHC panel produced using microarray data from ImmGen (http://www.immgen.org) (20). Rows represent different immune cell populations grouped by cell type. Columns represent genes.

expressed by splenic B cells and macrophages, we first stained for B cell and macrophage markers, Pax5 and CD163, respectively. By combining CD163 and Pax5 signal with the same chromogen or fluorophore, we demonstrate the effective use of a "dump channel" applied in an IHC setting (Fig. 3C, 3D). Staining for MHCII second with a different chromagen or fluorophore revealed a distinct population of $MHCII^{+}Pax5^{-}CD163^{-}$ cells, which we believe to be DCs (Fig. 3C, 3D).

Next, we developed a strategy to distinguish neutrophils from macrophages. Using knowledge from the literature and considering the available Abs for mouse targets, we stained for CD163 and FcgR4. According to ImmGen (Fig. 1) (20) and previous reports (16, 17), *FcgR4* is expressed by macrophages and neutrophils. This is corroborated by flow cytometric analysis (Fig. 3G). Based on this information, we expect that splenic macrophages are $CD163^{+}FcgR4^{+}$ and neutrophils are $CD163^{-}FcgR4^{+}$. Performing this multiplex staining reveals cells that follow these staining patterns (Fig. 3H, 3I).

Finally, we tested our immune panels and multiplex staining on 4T1 tumors, which is an immune cell–heavy model of breast cancer. We did multiplex IHC staining using chromogen and fluorescence detection methods (Fig. 4). Fig. 4A and 4B shows $CD3^{+}CD4^{+}$ and $CD3^{+}CD8^{+}$ T cells. We also detected $CD3^{-}CD4^{+}$ and $CD3^{-}CD8^{+}$ cells, which may be NK cells or DCs. Notably, all $CD3^{+}$ T cells were labeled with either CD4 or CD8, demonstrating the specificity and sensitivity of the staining, as the presence of double-negative or double-positive T lineage cells is unreported in this model.

Fig. 4D (inset, right arrow) shows the presence of $CD11c^{+}$ macrophages. This corresponds to tumor-associated macrophages, as resident tissue macrophages in the mammary fat pad are $CD11c^{-}$ (28). We also detected $F4/80^{-}CD163^{-}CD11c^{+}MHCII^{+}$ DCs (Fig. 4D, inset, left arrow).

Fig. 4G and 4H quantitation of different immune cell types in 4T1 tumors normalized to the DAPI signal. The 4T1 tumors have been reported to have high neutrophil infiltration (29). Consistent with this, our analysis shows a high frequency of $F4/80^{-}CD163^{-}FcgR4^{+}$ cells, which are presumably neutrophils (Fig. 4E, 4F).

Comparatively, we also found modest numbers of tissue macrophages ($F4/80^{+}CD163^{+}CD11c^{-}$), DCs ($F4/80^{-}CD163^{-}CD11c^{+}MHCII^{+}$), and T cells ($CD3^{+}CD4^{+}$ and $CD3^{+}CD8^{+}$), data that are consistent with the findings of other groups (30–32). In sum, these data illustrate how an

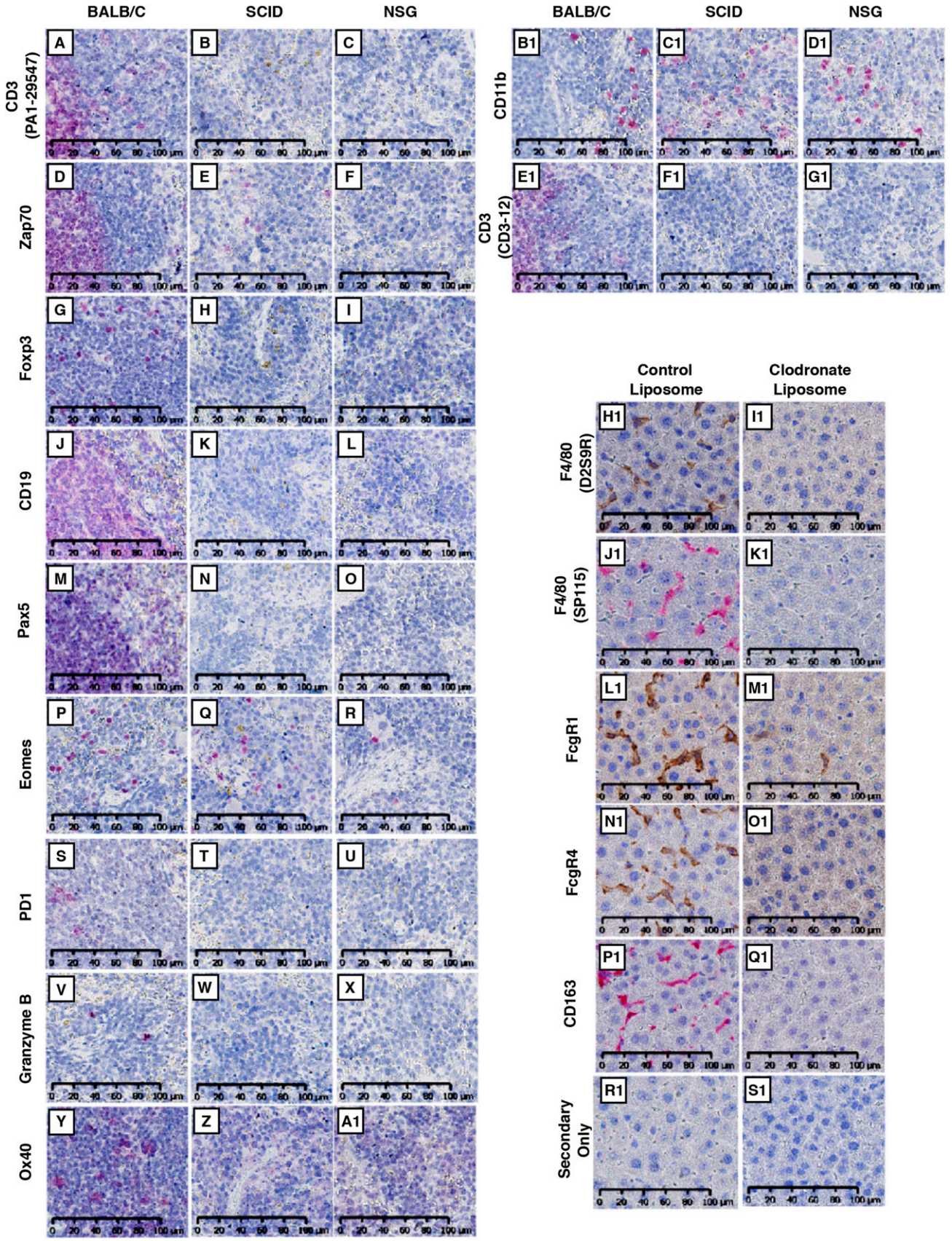

FIGURE 2. Validation of Ab specificity. (**A–G1**) Wild-type BALB/c, SCID, or NSG spleens were probed with Abs specific for CD3 [PA1-29547; (A–C)], Zap70 (D–F), Foxp3 (G–I), CD19 (J–L), Pax5 (M–O), Eomes (P–R), PD1(S–U), Granzyme B (V–X), Ox40 (Y–A1), CD11b (B1–D1), and CD3 [CD3-12; (E1– G1]. For detection, Warp Red chromogenic substrate was used. Slides were counterstained with hematoxylin and scanned at 20× using Hamamatsu NanoZoomer 2.0-HT. (**H1–S1**) Livers from control- or clodronate liposome–treated BALB/c mice were stained for F4/80 [D2S9R and SP115; (H1–K1), respectively], FcgR1 (L1 and M1), FcgR4 (N1 and O1), CD163 (P1 and Q1), or secondary only (R1 and S1). Slides were scanned at 20× using the Hamamatsu NanoZoomer 2.0-HT. All images represent a 40× field of view. Scale bar, 100 μm for all images.

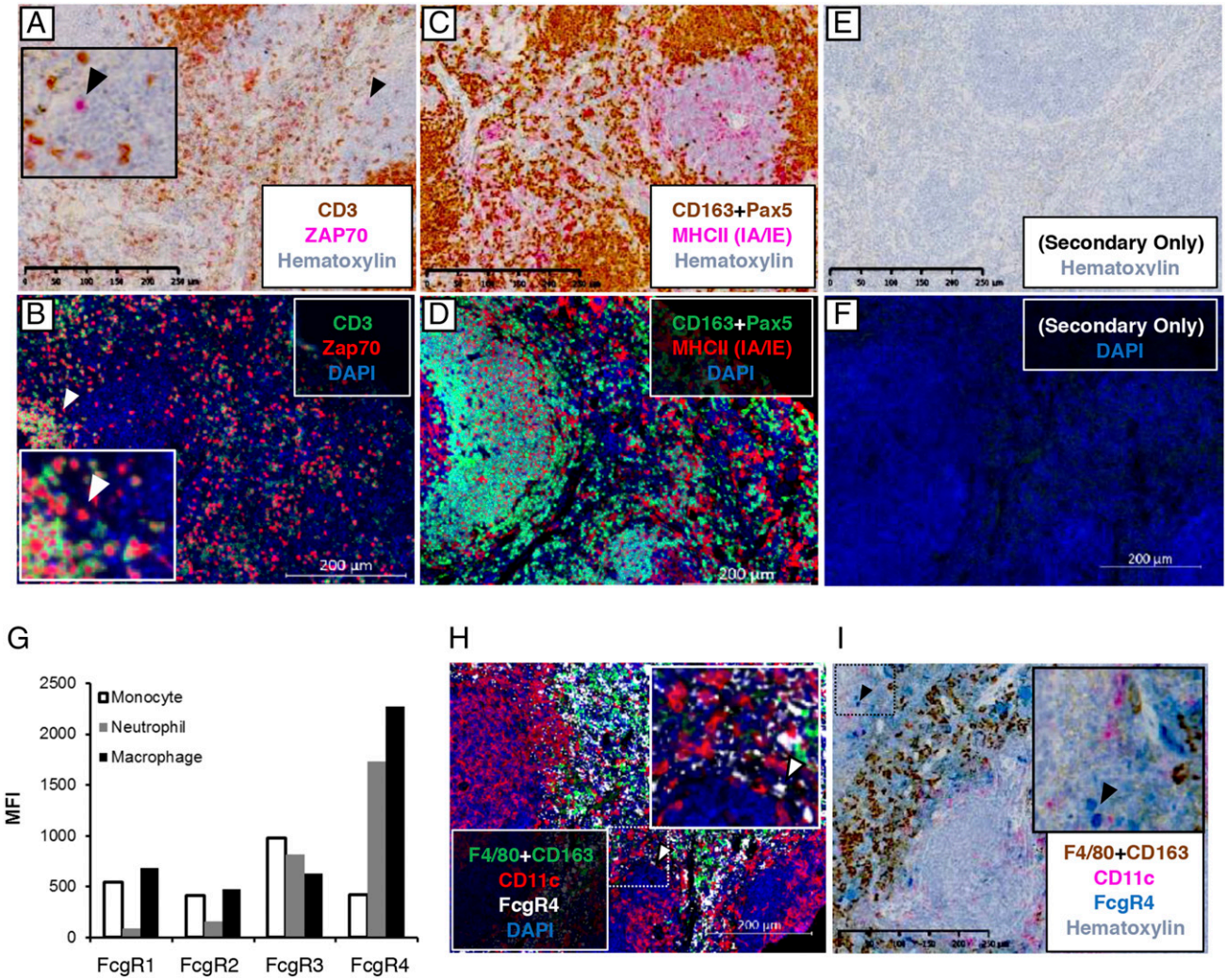

FIGURE 3. Multiplex IHC to stain NK cells, DCs, and neutrophils. BALB/c spleens were stained for (**A** and **B**) CD3 (PA1-29547, T cells) and Zap70 (T cells and NK cells); (**C** and **D**) Pax5 (B cells), CD163 (splenic macrophages), and MHCII (IA/IE); (**H** and **I**) F4/80 (SP115), CD163, CD11c, and FcgR4. (**E** and **F**) Secondary Ab only (without addition of primary Ab) was used for negative controls. Chromogenic substrates used were Betazoid DAB (brown) and Warp Red (pink). Opal 520 (green), Opal 570 (red), and Opal 690 (white) were used for fluorescence detection. Chromogen-stained sections were counterstained with hematoxylin. For fluorescence detection, sections were counterstained with DAPI (blue). Slides were scanned at 20× using the Hamamatsu NanoZoomer 2.0-HT (chromagen detection) or the Zeiss Axio Scan.Z1 (fluorescence detection). Images represent a 10× field of view. (**G**) Total splenocytes were isolated from C57BL/6 mice. FcgR expression was evaluated on neutrophils ($CD11b^+Ly6G^+Ly6C^-$), macrophages ($F4/80^+$), and monocytes ($CD11b^+Ly6c^+Ly6G^-$). FcgR signal is represented by mean fluorescence intensity. Scale bar, 250 μm for chromagen-stained images. Scale bar, 200 μm for fluorescent images.

effective multiplex IHC strategy can be exploited to investigate the immune dynamics of the tumor microenvironment.

Discussion

In this study, we produced a modified FFPE IHC protocol for mouse tissue that provides a more effective Ag retrieval method. Ag retrieval has been a longstanding challenge in the field, often requiring different retrieval protocols for different epitopes (14, 33, 34). Our protocol works consistently well for all of the Abs tested. The use of glycerol in the Tris/EDTA Ag retrieval buffer greatly increases the detection of multiple Ags and may be a better standard for mouse FFPE tissues. Also, the use of EDTA in the wash buffers prevents degradation of DNA by nucleases, preserving nuclear morphology, a consideration that is absent in other multiplex protocols. Finally, we found that treatment with 10% formalin immediately prior to Ag retrieval helps to maintain tissue integrity and reduces loss of tissue during multiple rounds of stripping and reprobing.

We also propose a novel strategy of using multiple markers to stain for cell types for which unique markers/Abs have not been identified or are not available commercially. This strategy can be particularly helpful to identify DCs, neutrophils, and NK cells in the tumor microenvironment. With new emerging immune regulators (35) and therapies, this strategy provides an excellent tool to investigate the effect of drug treatment and prognosis of disease.

Overall, our protocol of multiplex IHC staining on mouse tissue provides an improved strategy for reproducible staining. Using our strategy, and by properly planning the sequence of target Abs, visualization of multiple epitopes is only limited by the number of filter channels in the microscope. This protocol has the potential to improve the utility of multiplex IHC to investigate the immune system in vivo, including the analysis of the tumor immune microenvironment and mechanisms of action of immune-related drugs in preclinical models.

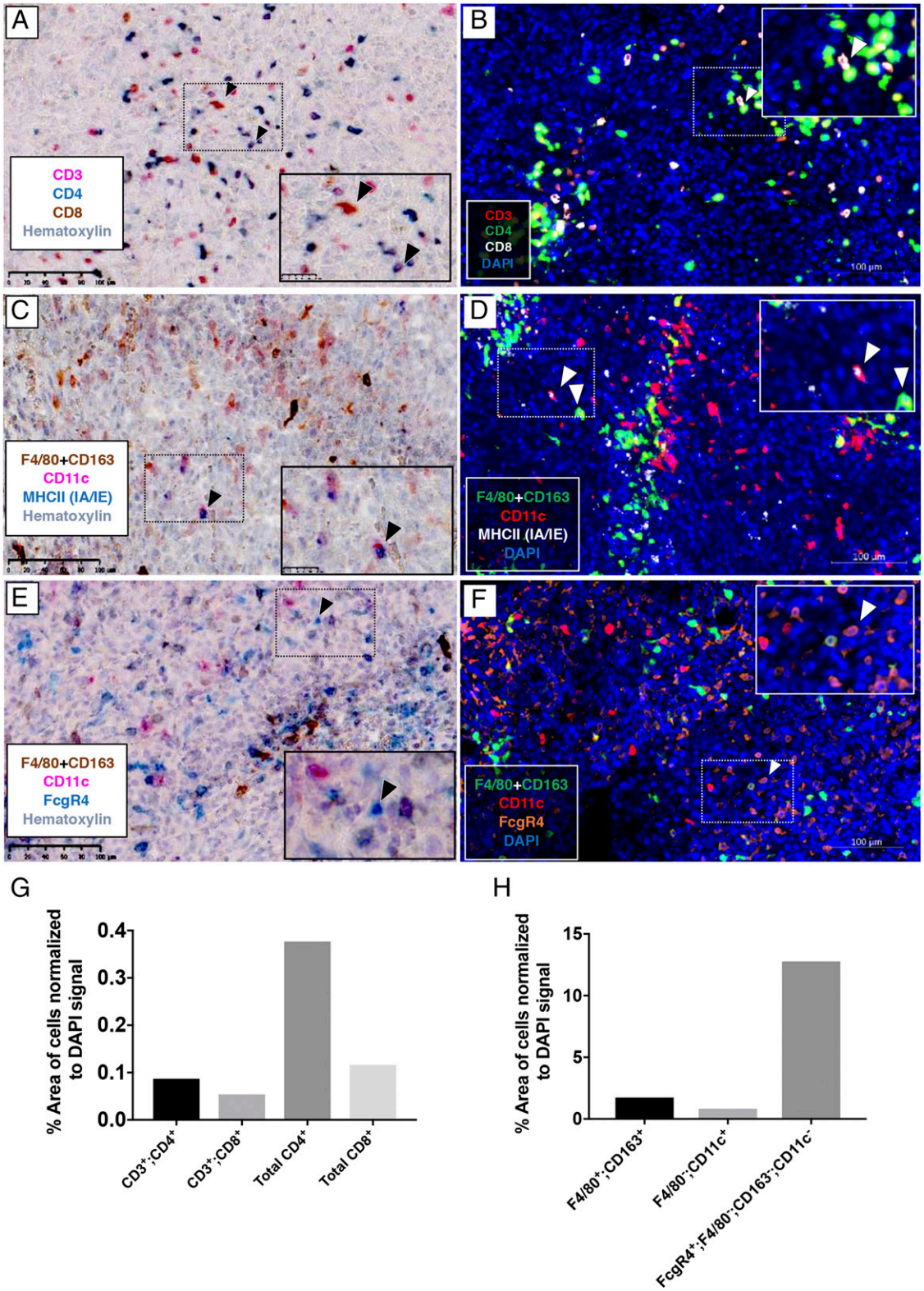

FIGURE 4. Multiplex IHC staining of 4T1 tumor tissues. The 4T1 primary tumors were stained for (**A** and **B**) CD3 (PA1-29547; T cells), CD4 (EPR19514; T cells, NK cells, and DCs), and CD8 (T cells, NK cells, and DCs); (**C** and **D**) CD11c, MHCII (IA/IE), CD163, and F4/80 (SP115) (**E** and **F**) CD11c, FcgR4, CD163, and F4/80 (SP115). Chromogenic substrates used were Betazoid DAB (brown), Warp Red (pink), and Feranji Blue (blue) (A, C, and E). Opal 520 (green), Opal 570 (red), and Opal 690 (white or orange) were used for fluorescent staining (B, D, and F). Chromogen sections were counterstained with hematoxylin, whereas DAPI staining was used for fluorescence detection. Slides were scanned at 20× using the Hamamatsu NanoZoomer 2.0-HT (chromagen detection) or the Zeiss Axio Scan.Z1 (fluorescence detection). Images represent a 20× field of view. Inset: higher magnification. (B–D) Arrows point to $CD3^+CD8^+$ (B), $CD11c^+MHCII^+$ [(C); (D), left arrow], or $CD163/F4/80^+CD11c^+$ cells [(D), right arrow]. (E and F) Arrows point to $FcgR4^+CD11c^-CD163/F4/80^-$ cells. (**G** and **H**) Cell types in 4T1 tumor sections were quantitated as percentage of area of positive cells normalized to DAPI signal. Scale bar, 100 µm for all images.

Acknowledgments

We thank D. Primm for editorial assistance and Drs. E. Koay and A. Zijlstra and members of the Brekken Laboratory for advice and helpful discussion.

Disclosures

The authors have no financial conflicts of interest.

References

1. Szánthó, E., B. Kárai, G. Ivády, J. Bedekovics, I. Szegedi, M. Petrás, G. Ujj, A. Ujfalusi, C. Kiss, J. Kappelmayer, and Z. Hevessy. 2018. Comparative analysis of multicolor flow cytometry and immunohistochemistry for the detection of disseminated tumor cells. *Appl. Immunohistochem. Mol. Morphol.* 26: 305–315.
2. Saravanan, L., and S. Juneja. 2010. Immunohistochemistry is a more sensitive marker for the detection of myeloperoxidase in acute myeloid leukemia compared with flow cytometry and cytochemistry. *Int. J. Lab. Hematol.* 32: e132–e136.
3. Koyama, S., E. A. Akbay, Y. Y. Li, A. R. Aref, F. Skoulidis, G. S. Herter-Sprie, K. A. Buczkowski, Y. Liu, M. M. Awad, W. L. Denning, et al. 2016. STK11/LKB1 deficiency promotes neutrophil recruitment and proinflammatory cytokine production to suppress T-cell activity in the lung tumor microenvironment. *Cancer Res.* 76: 999–1008.
4. Sridharan, V., E. Gjini, X. Liao, N. G. Chau, R. I. Haddad, M. Severgnini, P. Hammerman, A. El-Naggar, G. J. Freeman, F. S. Hodi, et al. 2016. Immune profiling of adenoid cystic carcinoma: PD-L2 expression and associations with tumor-infiltrating lymphocytes. *Cancer Immunol. Res.* 4: 679–687.
5. Ludwig, K. F., W. Du, N. B. Sorrelle, K. Wnuk-Lipinska, M. Topalovski, J. E. Toombs, V. H. Cruz, S. Yabuuchi, N. V. Rajeshkumar, A. Maitra, et al. 2018. Small-molecule inhibition of axl targets tumor immune suppression and enhances chemotherapy in pancreatic cancer. *Cancer Res.* 78: 246–255.
6. Erdag, G., J. T. Schaefer, M. E. Smolkin, D. H. Deacon, S. M. Shea, L. T. Dengel, J. W. Patterson, and C. L. Slingluff, Jr. 2012. Immunotype and immunohistologic characteristics of tumor-infiltrating immune cells are associated with clinical outcome in metastatic melanoma. *Cancer Res.* 72: 1070–1080.
7. Headley, M. B., A. Bins, A. Nip, E. W. Roberts, M. R. Looney, A. Gerard, and M. F. Krummel. 2016. Visualization of immediate immune responses to pioneer metastatic cells in the lung. *Nature* 531: 513–517.
8. Parra, E. R., N. Uraoka, M. Jiang, P. Cook, D. Gibbons, M. A. Forget, C. Bernatchez, C. Haymaker, I. I. Wistuba, and J. Rodriguez-Canales. 2017. Validation of multiplex immunofluorescence panels using multispectral microscopy for immune-profiling of formalin-fixed and paraffin-embedded human tumor tissues. *Sci. Rep.* 7: 13380.
9. Stack, E. C., C. Wang, K. A. Roman, and C. C. Hoyt. 2014. Multiplexed immunohistochemistry, imaging, and quantitation: a review, with an assessment of Tyramide signal amplification, multispectral imaging and multiplex analysis. *Methods* 70: 46–58.
10. Dixon, A. R., C. Bathany, M. Tsuei, J. White, K. F. Barald, and S. Takayama. 2015. Recent developments in multiplexing techniques for immunohistochemistry. *Expert Rev. Mol. Diagn.* 15: 1171–1186.
11. Hofman, F. M., and C. R. Taylor. 2013. Immunohistochemistry. *Curr. Protoc. Immunol.* 103: 21.4.1–21.4.26.
12. Wagrowska-Danilewicz, M., and M. Danilewicz. 2009. Immunofluorescence on paraffin-embedded sections in evaluation of immune complex deposits in renal biopsy specimens. *Pol. J. Pathol.* 60: 3–9.
13. Beckstead, J. H. 1994. A simple technique for preservation of fixation-sensitive antigens in paraffin-embedded tissues. *J. Histochem. Cytochem.* 42: 1127–1134.
14. Feng, Z., S. M. Jensen, D. J. Messenheimer, M. Farhad, M. Neuberger, C. B. Bifulco, and B. A. Fox. 2016. Multispectral imaging of T and B cells in murine spleen and tumor. [Published erratum appears in 2017 *J. Immunol.* 198: 1759.] *J. Immunol.* 196: 3943–3950.
15. Lykidis, D., S. Van Noorden, A. Armstrong, B. Spencer-Dene, J. Li, Z. Zhuang, and G. W. Stamp. 2007. Novel zinc-based fixative for high quality DNA, RNA and protein analysis. *Nucleic Acids Res.* 35: e85.
16. Tutt, A. L., S. James, S. A. Laversin, T. R. Tipton, M. Ashton-Key, R. R. French, K. Hussain, A. T. Vaughan, L. Dou, A. Earley, et al. 2015. Development and characterization of monoclonal antibodies specific for mouse and human Fcγ receptors. *J. Immunol.* 195: 5503–5516.
17. Dahal, L. N., A. Gadd, A. D. Edwards, M. S. Cragg, and S. A. Beers. 2018. UC-1V150, a potent TLR7 agonist capable of activating macrophages and potentiating mAb-mediated target cell deletion. *Scand. J. Immunol.* 87: e12666.
18. Schindelin, J., I. Arganda-Carreras, E. Frise, V. Kaynig, M. Longair, T. Pietzsch, S. Preibisch, C. Rueden, S. Saalfeld, B. Schmid, et al. 2012. Fiji: an open-source platform for biological-image analysis. *Nat. Methods* 9: 676–682.
19. Pileri, S. A., G. Roncador, C. Ceccarelli, M. Piccioli, A. Briskomatis, E. Sabattini, S. Ascani, D. Santini, P. P. Piccaluga, O. Leone, et al. 1997. Antigen retrieval techniques in immunohistochemistry: comparison of different methods. *J. Pathol.* 183: 116–123.
20. Immunological Genome Project Consortium. 2008. The Immunological Genome Project: networks of gene expression in immune cells. *Nat. Immunol.* 9: 1091–1094.
21. Au-Yeung, B. B., S. Deindl, L. Y. Hsu, E. H. Palacios, S. E. Levin, J. Kuriyan, and A. Weiss. 2009. The structure, regulation, and function of ZAP-70. *Immunol. Rev.* 228: 41–57.
22. Shiraishi, D., Y. Fujiwara, H. Horlad, Y. Saito, T. Iriki, J. Tsuboki, P. Cheng, N. Nakagata, H. Mizuta, H. Bekki, et al. 2018. CD163 is required for protumoral activation of macrophages in human and murine sarcoma. *Cancer Res.* 78: 3255–3266.
23. Gabrilovich, D. I., S. Ostrand-Rosenberg, and V. Bronte. 2012. Coordinated regulation of myeloid cells by tumours. *Nat. Rev. Immunol.* 12: 253–268.
24. Cobaleda, C., A. Schebesta, A. Delogu, and M. Busslinger. 2007. Pax5: the guardian of B cell identity and function. *Nat. Immunol.* 8: 463–470.
25. Bronte, V., and M. J. Pittet. 2013. The spleen in local and systemic regulation of immunity. *Immunity* 39: 806–818.
26. Claassen, E., and N. Van Rooijen. 1984. The effect of elimination of macrophages on the tissue distribution of liposomes containing [3H]methotrexate. *Biochim. Biophys. Acta* 802: 428–434.
27. Seiler, P., P. Aichele, B. Odermatt, H. Hengartner, R. M. Zinkernagel, and R. A. Schwendener. 1997. Crucial role of marginal zone macrophages and marginal zone metallophils in the clearance of lymphocytic choriomeningitis virus infection. *Eur. J. Immunol.* 27: 2626–2633.
28. Franklin, R. A., W. Liao, A. Sarkar, M. V. Kim, M. R. Bivona, K. Liu, E. G. Pamer, and M. O. Li. 2014. The cellular and molecular origin of tumor-associated macrophages. *Science* 344: 921–925.
29. Park, J., R. W. Wysocki, Z. Amoozgar, L. Maiorino, M. R. Fein, J. Jorns, A. F. Schott, Y. Kinugasa-Katayama, Y. Lee, N. H. Won, et al. 2016. Cancer cells induce metastasis-supporting neutrophil extracellular DNA traps. *Sci. Transl. Med.* 8: 361ra138.
30. Huang, Y., C. Ma, Q. Zhang, J. Ye, F. Wang, Y. Zhang, P. Hunborg, M. A. Varvares, D. F. Hoft, E. C. Hsueh, and G. Peng. 2015. CD4+ and CD8+ T cells have opposing roles in breast cancer progression and outcome. *Oncotarget* 6: 17462–17478.
31. Song, H., J. I. Jung, H. J. Cho, S. Her, S. H. Kwon, R. Yu, Y. H. Kang, K. W. Lee, and J. H. Park. 2015. Inhibition of tumor progression by oral piceatannol in mouse 4T1 mammary cancer is associated with decreased angiogenesis and macrophage infiltration. *J. Nutr. Biochem.* 26: 1368–1378.
32. Roland, C. L., K. D. Lynn, J. E. Toombs, S. P. Dineen, D. G. Udugamasooriya, and R. A. Brekken. 2009. Cytokine levels correlate with immune cell infiltration after anti-VEGF therapy in preclinical mouse models of breast cancer. *PLoS One* 4: e7669.
33. Shi, S. R., M. E. Key, and K. L. Kalra. 1991. Antigen retrieval in formalin-fixed, paraffin-embedded tissues: an enhancement method for immunohistochemical staining based on microwave oven heating of tissue sections. *J. Histochem. Cytochem.* 39: 741–748.
34. Shi, S. R., C. Liu, and C. R. Taylor. 2007. Standardization of immunohistochemistry for formalin-fixed, paraffin-embedded tissue sections based on the antigen-retrieval technique: from experiments to hypothesis. *J. Histochem. Cytochem.* 55: 105–109.
35. Sorrelle, N., A. T. A. Dominguez, and R. A. Brekken. 2017. From top to bottom: midkine and pleiotrophin as emerging players in immune regulation. *J. Leukoc. Biol.* 102: 277–286.